

# Three-Dimensional Microfabrication by Localized Electrochemical Deposition

John D. Madden and Ian W. Hunter

**Abstract**—A microfabrication technology capable of electrodepositing truly three-dimensional metal structures is introduced. Micrometer-scale nickel structures including a multicoiled helical spring have been fabricated. Electrodeposition is localized by placing a sharp-tipped electrode in a plating solution, near a substrate, and applying a voltage. Structures are built by moving the electrode appropriately with respect to the substrate. Vertical deposition rates of 6  $\mu\text{m/s}$  are observed, two orders of magnitude greater than those of conventional electrodeposition. The theory of mass transport to a region of localized field is discussed, and a model of deposition profile is presented. The process can potentially produce submicrometer feature sizes using a range of materials including pure metals, alloys, and polymers. [121]

## I. INTRODUCTION

**F**ABRICATION techniques currently employed to construct microelectromechanical systems are largely derived from microelectronics technology. Clearly, the technology is highly developed and is well suited for mass production. Silicon, the material employed by many of the techniques, has favorable mechanical and electrical properties [1]. However, the structures produced using microelectronics methods are largely of low aspect ratio (height to width) and often limited to the use of silicon. Such structures do not optimize functionality for many applications. Furthermore, equipment is generally expensive, and long development times, on the order of years, are not uncommon. Small- and medium-scale markets are thus inaccessible, except where a premium will be paid for size, and rapid prototyping is difficult. Therefore, we feel that it is important to investigate alternative microfabrication methods that are capable of producing three-dimensional (3-D) micro-structures from a range of materials and preferably at low cost. Our particular motivation stems from an endeavor to extend the capabilities of our micro-surgical robots [2], a task wherein a 3-D fabrication capability, a range of available materials, and rapid prototyping are all highly desirable.

Lithography, electroforming, and molding (LIGA) [3], [4] and other photolithography-related processes [5] address the aspect ratio problem by employing deep resist layers. As a result, thick structures are produced that have lateral, but no vertical, features. Multilayers are possible, resulting in vertical steps [4], [6], but there is a trade-off between aspect ratio,

Manuscript received August 2, 1994; revised October 24, 1995. Subject Editor, R. O. Warrington. This work was supported in part through the Institute of Robotics and Intelligent Systems, Canada, and the U.S. Office of Naval Research. J. D. Madden was supported by a National Science and Engineering Research Council of Canada scholarship.

The authors are with the Department of Mechanical Engineering, Massachusetts Institute of Technology, Cambridge MA 02139 USA.

Publisher Item Identifier S 1057-7157(96)01464-3.

which is maximized by employing thick layers, and feature size in the vertical direction, which is clearly improved by reducing the step size. LIGA and related procedures can produce gears and microrotors, but vesicles, helices, and curved pipes are difficult or impossible to fabricate.

Material removal methods such as excimer laser machining [7], electrical discharge machining [8], and ion beam milling [9] are becoming effective construction tools on micrometer scales, but they lack the geometric versatility of formation by selective material deposition and are constrained to the properties of the material chosen to machine. By selectively depositing material, as in laying bricks or icing a cake, objects of virtually arbitrary geometry can be formed.

From the standpoint of geometrical capability, material deposition techniques are attractive. Several techniques are under development, the most notable being laser-assisted chemical vapour deposition (LCVD) [10] and ultraviolet stereo lithography [11], both of which make use of the interaction of focused light beams with matter to form 3-D objects. LCVD has produced helical springs, and stereo lithography is capable of forming helices and bent pipes. However, LCVD [12] and stereo lithography are unlikely to produce submicrometer features in their present forms due to diffraction limitation and thermal conduction. Furthermore, both are limited in the materials available, stereo lithography in particular currently being limited to the deposition of UV sensitive polymers. By employing the polymer structures as molds, however, 3-D metal structures can be built.

Localized chemical vapour deposition with submicrometer resolution can be achieved using focused electron [13] and ion [14] beams, replacing the laser employed in LCVD. These can also be used to remove material. While resolution is high, vertical deposition rates are low ( $\sim 20$  nm/s using electrons and  $\sim 1$  nm/s with ions).

Electrodeposition is attractive because many materials can be deposited, including metals, metal alloys, conducting polymers and even some semiconductors [15]. Furthermore, it has been demonstrated that submicrometer metal lines [16] and micrometer-wide polymer lines [17] can be electrodeposited on a surface. Finally, while conventional plating is limited to vertical deposition rates on the order of 30 nm/s, localized deposition has been achieved at rates of greater than 30  $\mu\text{m/s}$  [18].

In order to produce localized deposition on a surface, one approach is to place a microelectrode near a conducting substrate and to apply a potential between the two through a plating solution [16], [17]. The electric field is localized to the

region between the microelectrode and the substrate, which in turn localizes the deposit. The microelectrode is scanned along the surface to produce thin lines of deposited material. Electrochemical etching has also been achieved using this process [19].

In this paper we demonstrate the fabrication of 3-D structures by moving the microelectrode in three dimensions rather than two. The process of 3-D localized electrochemical deposition is now introduced, the theory of deposition is outlined, and the first micrometer scale structures are described.

## II. THEORY

### A. Concept

The process involves localized electrochemical deposition (Fig. 1). The tip of a sharp pointed electrode is placed in a plating solution and brought near the surface where deposition is to occur. Potential is applied between the tip and the substrate. Electric field, and thus deposition, are confined to the region beneath the tip, as demonstrated in Fig. 1(a). The tip is then moved with respect to the forming surface to create structures [Fig. 1(b)]. In principle the size of the electrode determines the spatial resolution and any structure geometry is possible, providing it is electrically continuous with the substrate. The electrochemical nature not only allows deposition but also etching and polishing.

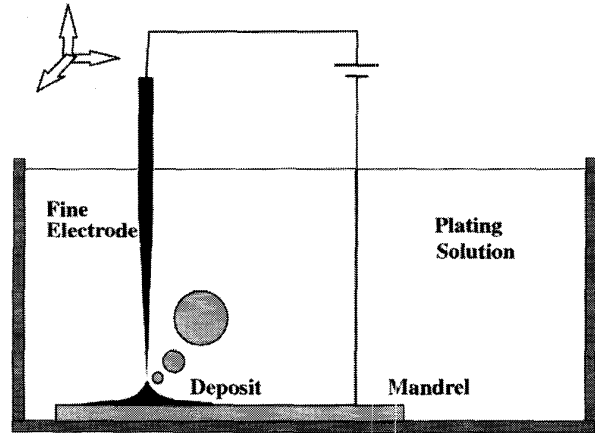
Various phenomena affect the deposition of ions from solution onto a substrate including mass transport, electron transfer, electrical potential, chemical potential, and crystal growth [20]. In metal deposition for example, an ion must reach the electrode/solution interface, receive electrons to become an atom, and then join other atoms to form a crystal. These stages are discussed in order to give an understanding of the factors affecting deposition rate and profile.

### B. Deposition Rate

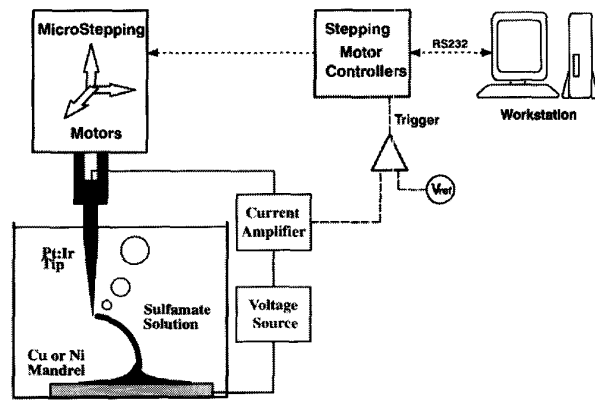
Conventional electroplating rates are too slow to make a localized electrochemical deposition process feasible. Study of the limiting processes, however, suggests means of enhancing rate. Electron transfer and mass transport are generally the main factors affecting the rate of electrodeposition [20].

**Electron Transfer:** At equilibrium, a balance between chemical and electrical potential occurs at the electrode/solution interface manifesting itself as an  $\sim 1$  to 30-nm-thick charged region known as the double layer [21], [22]. To achieve electron transfer, an activation energy is required for an ion or molecule to rid itself of solvating molecules, travel through the double layer, and adjust its hydration sphere for electron transfer. An equal energy is required for atoms and molecules leaving the surface, and a dynamic equilibrium exists with oxidation and reduction currents matching each other. If the electrical potential is changed from the equilibrium value by an amount,  $\eta$ , either reduction or oxidation is favored, as described by the semi-empirical Butler-Volmer equation [21]

$$j = j_o [e^{(1-\alpha)f\eta} - e^{-\alpha f\eta}] \quad (1)$$



(a)



(b)

Fig. 1. (a) The concept of localized electrochemical deposition. (b) The apparatus including the current feedback loop used for position control.

where

$$f = \frac{F}{RT}$$

and  $j$  is current density,  $j_o$  is exchange current density (the absolute value of the oxidation or reduction current at equilibrium),  $F$  is one Faraday ( $9.6485 \times 10^4 \text{ C mol}^{-1}$ ),  $R$  is the gas constant ( $8.31451 \text{ JK}^{-1} \text{ mol}^{-1}$ ),  $T$  is the absolute temperature, and  $\alpha$  is an experimentally derived parameter known as the transfer coefficient, which lies between zero and one and is usually  $\sim 0.5$ . Once overpotential exceeds  $\sim 100 \text{ mV}$ , the rate of transfer rises exponentially (assuming  $\alpha = 0.5$ ). At the potentials used in electroplating and forming, electron transfer rates generally greatly exceed those of mass transport. The concentration of the reactant is reduced near the electrode and mass transport is the rate determining step.

**Mass Transport:** The three mechanisms of mass transport are diffusion, migration, and convection. Diffusion is driven by concentration gradients, migration by the action of electrical potential gradients on charges, and convection by pressure gradients [22].

*Diffusion:* In conventional electroplating and forming, diffusion is the rate determining process [23]. The concentration gradients created by the much more rapid process of electron transfer at the electrode induce diffusion. Rates of diffusion can be increased by reducing electrode diameter. As electrode diameter is reduced, the depleted volume has a cubic dependence on diameter, while the surface area decreases only with the square. Current density,  $j$ , is thus a function of electrode radius,  $r_o$ , as well as the diffusion coefficient,  $D_o$ , bulk concentration,  $C_o$ , and the number of electrons reduced or oxidized per molecule,  $n$  [24]

$$j(r_o, t \rightarrow \infty) = \frac{nFD_oC_o}{r_o} \quad (2)$$

for a hemispherical electrode. The concentration,  $C$ , as a function of radius,  $r$ , at steady state is

$$C(r, t \rightarrow \infty) = C_o \left(1 - \frac{r_o}{r}\right). \quad (3)$$

Current density at a disk electrode behaves identically, but with a different geometry-related constant. Reducing the electrode diameter from 100  $\mu\text{m}$  to 0.1  $\mu\text{m}$  increases diffusion current by 1000 times. For a sulfamate solution, for example, as used to build the nickel structures described below, this corresponds to a change in deposition rate from 0.06  $\mu\text{m/s}$  to 60  $\mu\text{m/s}$ , making localized deposition feasible using <5- $\mu\text{m}$ -diameter electrodes. Note that while vertical deposition rate is inversely proportional to electrode diameter, the rate of volume deposition is directly proportional to diameter for a diffusion-limited process. In situations where fabrication rate is diffusion limited, one would ideally have a range of electrode sizes available to produce a range of feature sizes in the least time.

*Convection:* Depletion of ions near the electrode also creates density gradients between the depleted region and the electrode, resulting in natural convection. Agitation is often used to force convection, leading to the flow of bulk solution into the depletion layer and increasing deposition rates by as much as 100 times [20]. However, rapid nickel deposition rates, for example, are still only on the order of 0.03  $\mu\text{m/s}$  [25]. At such low rates, a serial deposition process, as is proposed here, is impractical.

Agitation reduces the depleted region from an initial value of as much as 500  $\mu\text{m}$  to  $\sim 10$   $\mu\text{m}$  [26]. In spite of agitation, deposition remains diffusion limited because viscous forces near the electrode surface impede the influx of fluid. Jet plating, in which fluid is fired at a surface through a nozzle, allows high rates of deposition (several  $\mu\text{m/s}$ ) local to the point at which the stream impacts the substrate surface [18]. Also, local heating of the surface can be used to create micro-stirring, bringing solution directly to the surface. A technique known as laser enhanced electroplating (LEEP) takes advantage of this effect by focusing a laser beam onto the plating surface [27], apparently resulting in convection both by the inducement of micro-stirring and, with sufficient laser intensity, by local boiling. Rates of deposition and etching are enhanced by more than three orders of magnitude over rates in an unagitated solution. Two-micrometer-wide lines have been deposited using this process and vertical deposition rates

of greater than 6  $\mu\text{m/s}$  achieved. However, LEEP appears to be impractical for 3-D fabrication because as the deposit thickness increases, so does thermal conduction away from the beam focal point, which results in increased feature size. Furthermore, the feature size is ultimately diffraction limited, making it unlikely to achieve a resolution of less than 1  $\mu\text{m}$  [28]. LEEP demonstrates, however, that flow at the surface can significantly increase deposition rates as required for a serial deposition process to be successful.

*Migration:* The current density,  $j$ , due to migration of a species in solution is proportional to the electric field,  $E$ , by Ohm's law [21]

$$j = \sigma E \quad (4)$$

with

$$\sigma = zuCF \quad (5)$$

where  $\sigma$  is conductivity,  $u$  is the ionic mobility, and  $z$  is the ionic charge. All charged species in solution are acted upon by the field, irrespective of whether they are involved in deposition or not, the proportion of current carried by a given species being specified by its transport number [22]. In conventional electrochemical configurations, migration generally plays a secondary role in mass transport to the depleted region because much of the current is carried by ions of species that do not react. In sulfamate solution—the nickel plating solution used to create the structures presented in this paper—the nickel ion transport number is estimated to be 0.25. (Note that the plating efficiency can still be 100%, providing only nickel ions react at the electrode surface.) In this case, diffusion and convection account for the transport of the remaining 75% of nickel ions to the interface.

When the field is localized using a microelectrode, very strong, localized fields are produced. This allows very high local rates of migration, but does not contribute to the influx of ions to the region between the microelectrode and the substrate. This may, in effect, contribute to depletion, adding to the dependence on other forms of mass transport.

*Deposition Profile:* Deposition profile refers to the geometry of the deposit produced by a given electrode configuration. In order to determine the deposition profile, the current density at the substrate surface must be calculated. This involves solving for mass transport, electron transfer, double-layer impedance, and the distribution of electrical potential,  $\Phi$ . We chose to begin with an estimate of the field distribution at the substrate due to a nearby microelectrode, since the electrical potential drives the electrochemical reaction and localization of electric field is the key to the localization of deposit in our configuration.

The distribution of electrical potential is given by Poisson's equation [29]

$$\nabla^2 \Phi = \frac{\rho}{\epsilon} \quad (6)$$

where  $\rho$  is charge density and  $\epsilon_o$  is the permittivity. In order to estimate the shape of the field, it is assumed that there is no net charge, reducing the problem to solving Laplace's

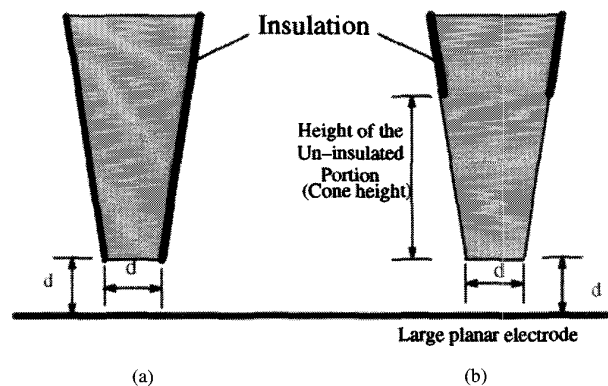


Fig. 2. Modeled electrode tip geometries. (a) Disk. (b) Disk and cone.

equation. The actual field profile will be distorted by double-layer charging. The double layer, however, is generally only between 1 and 30 nm thick.

Microelectrode geometry is modeled upon electrochemically etched electrodes, such as those used for scanning tunneling microscopy [30] and scanning electrochemical microscopy [31]. The etched tips generally have a conical shape converging to an approximately discoid or hemispherical point, as illustrated in Fig. 2. Two electrode configurations are modeled, one in which insulation covers the length of the electrode, leaving only a disk-shaped tip exposed, and secondly a configuration in which a portion of the conical segment above the disk is left uninsulated. The cone angle is  $28^\circ$ , the value chosen to be representative of cone angles in the etched tips. The model assumes that the disk electrode sits one disk diameter above and parallel to a much larger planar electrode for all configurations. This separation is chosen because the current at microelectrodes begins to rise from its bulk value as it approaches within a disk diameter of a large planar surface [32], suggesting a feedback mechanism for future servo control of tip position. A potential difference is applied between the microelectrode and the plane. Between the two lies a medium of constant conductivity. Calculations were done using a finite-element modeling package [33].

Fig. 3 shows the calculated field strength over a cross section perpendicular to the underlying plane and to the surface of the disk electrode. Note that the highest fields occur at the edge of the microelectrode, as expected. In Fig. 4(a) the field strength profile along the plane's surface is plotted for both the disk configuration and for cone heights that are 3, 10, and  $50\times$  the disk diameter. The full width at half maximum (FWHM) ranges between  $1.6\times$  the disk diameter for the disk alone, and  $\sim 2.3\times$  for the  $10\times$  and  $50\times$  cones, demonstrating that the field is effectively localized under the modeled conditions. Furthermore, profile broadening appears to be converging as cone height is increased, as expected given that spreading of the field lines and resistance both increase as electrode elements are placed further from the substrate. Thus, even sharp uninsulated electrodes should be effective in providing field localization.

Fig. 4(b) compares the observed deposition profiles with the model results of Fig. 4(a). To generate the observed profiles,

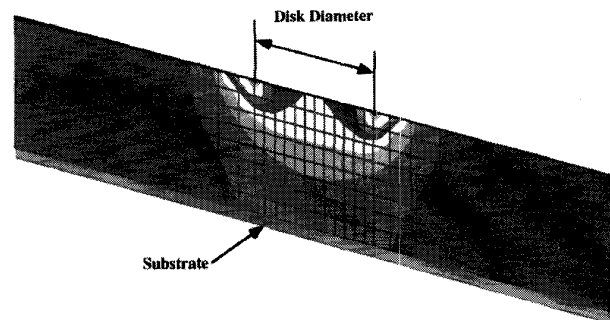


Fig. 3. Modeled cross section of current density between a circular disk and a planar substrate. Contours are spaced linearly representing a variation in field strength of  $150\times$ , the strongest fields being at the disk edge. Grid lines delineate the borders of the model elements used. Disk diameter: electrode-substrate separation = 1 : 1.

a  $500\text{-}\mu\text{m}$ -diameter platinum wire was cut, polished, and insulated (Crown Wax, S.S. White, Philadelphia, PA) to form the disk-shaped electrode employed. The electrode was placed one disk diameter above a copper substrate and a potential (4.2 V) was applied between the electrode and the substrate through a sulfamate nickel plating solution, described in the next section, generating profile 1 in Fig. 4(b). Forced convection from a syringe smoothed deposition, removing bubbles from the deposition region. Also shown in Fig. 4(b) is profile 2, generated under the same conditions but without the wax coating, with the naked wire immersed in  $\sim 6$  mm of solution. Profiles were obtained using a profilometer.

The shape of the modeled and observed disk electrode deposition profiles agree well, with the observed profile being slightly narrower. The model assumed a flat substrate, whereas, as deposition proceeds, material is successively deposited on an increasingly curved surface, concentrating field lines and thereby likely narrowing the profile.

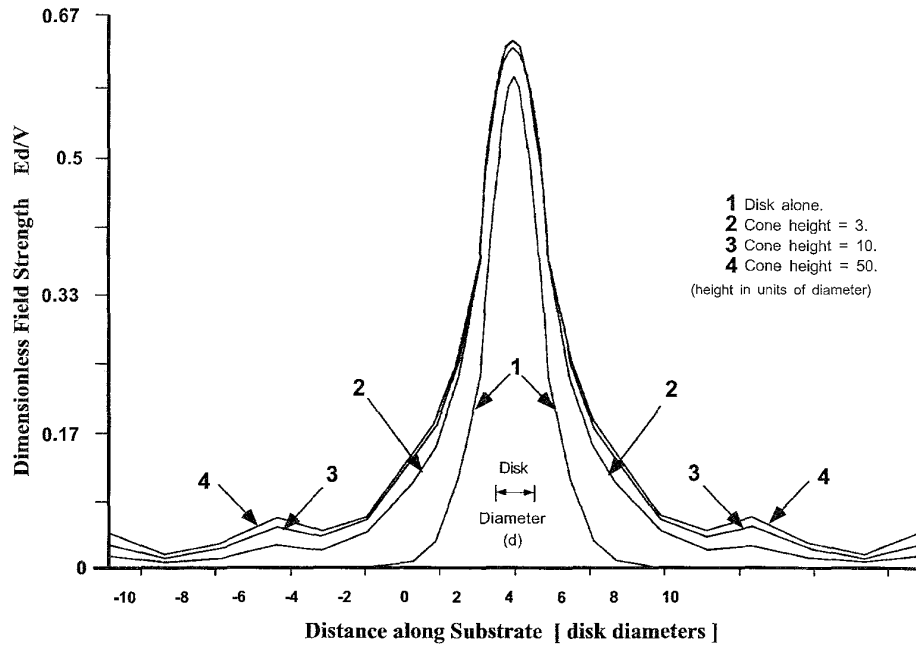
The wire electrode induced profile, curve 2 in Fig. 4(b), is higher than the disk profile, which is not surprising given that the wire presents more electrode surface area. It is much narrower at its base than the modeled cone electrode profile shown, which again is as expected given that the cone flares outwards, tending to increase the lateral spread.

The next two sections present the first structures built and include a comparison of tip geometry with structure dimension, confirming that deposition remains localized with electrode sizes in the tens of micrometers.

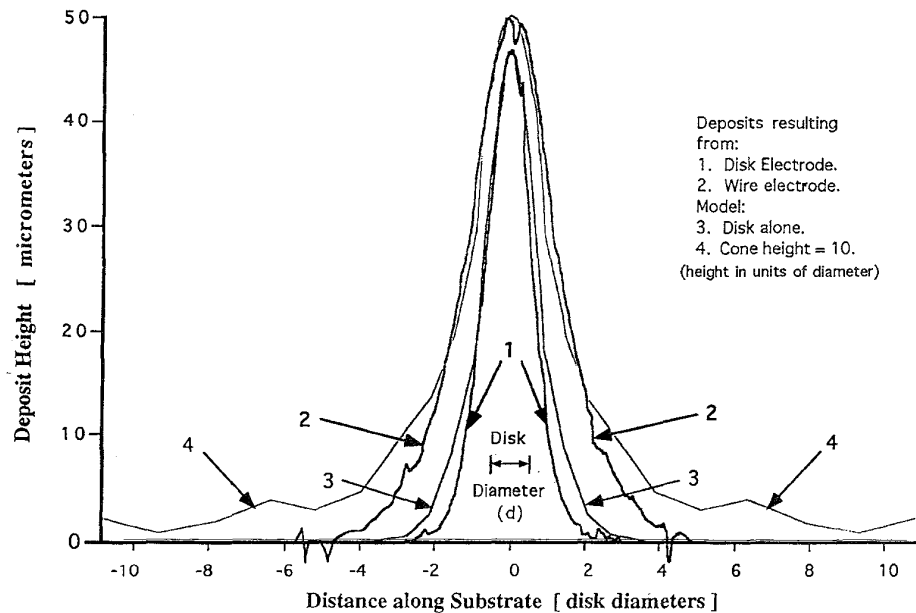
### III. EXPERIMENTAL METHODS

Fig. 1(b) is a schematic of the experimental configuration. Nickel structures were formed from a sulfamate solution [23],  $\text{Ni}(\text{SO}_3\text{NH}_2)_2$  :450g/L,  $\text{H}_3\text{BO}_3$  :30g/L (Aldrich, Milwaukee, WI) onto nickel or copper mandrels. Mandrel surfaces were mechanically polished down to finishes produced by using between 3 and  $0.3\text{-}\mu\text{m}$ -diameter alumina powder, as determined by the size of structure to be produced.

Three hundred- $\mu\text{m}$ -diameter platinum wires were electrochemically etched in a solution of saturated NaCl (36% by



(a)



(b)

Fig. 4. (a) Modeled magnitude of the electric field at the substrate surface, with field scaled by the disk diameter,  $d$ , and the applied potential,  $V$ . (b) Observed deposition profiles resulting from a Pt disk electrode ( $500\ \mu\text{m}$  diameter) and a Pt wire electrode ( $500\ \mu\text{m}$  diameter) compared with modeled profiles.

volume), HCl (4%), and water (60%) [34] against a graphite rod at 22 V RMS to form conical electrodes with 20 to  $100\text{-}\mu\text{m}$ -diameter tips. Etched and glass or Epoxylite 6001 (Epoxylite Corp., Irvine, CA) coated platinum + iridium electrodes with tip diameters between 5 and  $15\ \mu\text{m}$  (FHC Corp., Brunswick, ME) were also used.

Tips are translated in three dimensions using micro-stepping motors (M and A series, Compumotor Corp., Rohnert Park, CA) and stages (Design Components Inc, Medfield, MA). The motors are driven by microstep drives (AX series, 12 800 steps/revolution, Compumotor) allowing a  $0.1\ \mu\text{m}$  step size on each axis. ASCII commands sent from a workstation (IBM

RS/6000 320) to the drives determine the trajectory. The operator interacts with a custom graphical user interface to specify geometry.

A 4.5–5 V potential is applied between the tip and the substrate in the sulfamate solution to induce rapid deposition. In open-loop mode the tip velocity is constant. In closed-loop operation [Fig. 1(b)], current through the circuit is monitored (Keithley 428 current amplifier). Sharp rises in current ( $\sim 10\times$ ) indicate contact between the tip and the forming surface. These are used to trigger motion. Closed loop control is difficult using very fine uninsulated tips because of the high background current. Thus, coated electrodes were used. Electrodes are initially positioned at the substrate surface by applying a low voltage ( $\sim 1$  V) and lowering the tip until a sharp rise in current is observed.

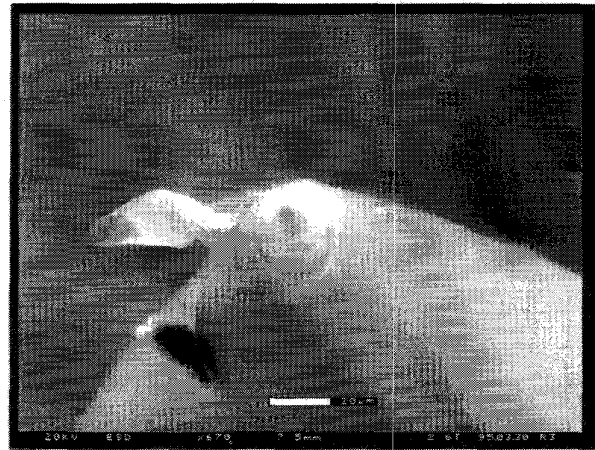
#### IV. RESULTS

Fig. 5 shows electron micrographs of an insulated, epoxy coated tip (a) before use, (b) after 5-min application of 5 V in solution, and (c) after building a 400- $\mu\text{m}$ -tall nickel column. Fig. 6 shows the column. Vigorous bubble formation occurring at the tip strips away insulation, as seen by comparing Fig. 5(a) and (b), where the width of the exposed tip region is increased from about 10  $\mu\text{m}$  to 25  $\mu\text{m}$ . Contact with the substrate surface appears to cause the flattening of the tip observed in Fig. 5(c). Flattening is reduced if the initial approach to contact the surface is made slowly ( $< 2$   $\mu\text{m}/\text{s}$ ) and the threshold contact current is set low. The tip diameter is about 45  $\mu\text{m}$ , the same as the column diameter. An energy-dispersive x-ray analysis of the tip atomic composition indicates that the contact between the tip and the deposit, used as feedback in the deposition process, does not result in material being fused to the tip.

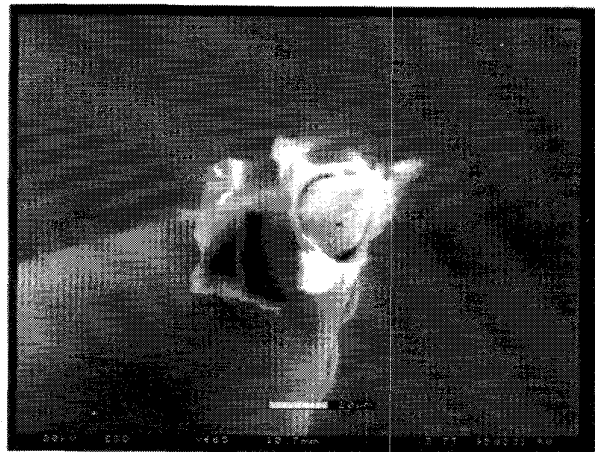
Note the striations perpendicular to the direction of growth seen in the column. These occur independent of whether feedback or constant velocity is employed to move the tip relative to the substrate. SEM observations suggest that during deposition a submicrometer-sized whisker grows up to contact the tip. It is speculated that the whisker eventually loses contact with the tip. When contact is broken, material then deposits around the whisker. Loss of contact between tip and substrate for up to one sec is occasionally observed.

Fig. 7 is an electron micrograph of a nickel column 100  $\mu\text{m}$  high and 10  $\mu\text{m}$  in diameter. The structure stands on a copper substrate and was constructed in closed-loop mode using a glass-coated electrode. The tip was moved vertically from the surface under servocontrol.

Fig. 8 shows a nickel spring constructed by spiraling an uninsulated Pt electrode upward at a constant speed of 6  $\mu\text{m}/\text{s}$ . The deposition rate is two orders of magnitude higher than that of conventional nickel electroforming. Diffusion at a 100- $\mu\text{m}$  electrode is two orders of magnitude too slow to account for the observed deposition rate, suggesting that convection is involved. We have observed that rapid deposition is accompanied by vigorous bubbling, which, as discussed above, has been shown to induce convection in laser-enhanced electroplating.



(a)



(b)



(c)

Fig. 5. (a) Epoxy-coated etched Pt:Ir wire. Note protruding metal tip. (b) Same tip after the application of 5 V between the tip and substrate in sulfamate solution. (c) Same tip after lowering to contact the substrate and depositing the structure shown in Fig. 6. Magnification is the same in all images.

Fig. 9 shows that the spring has a hollow core. It is hollow only on one side, and we suspect that the hollowness is due

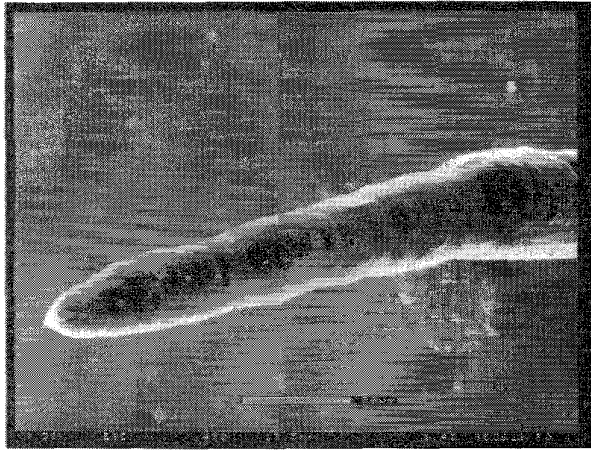


Fig. 6. Nickel column 45  $\mu\text{m}$  in diameter grown using tip shown in Fig. 5.

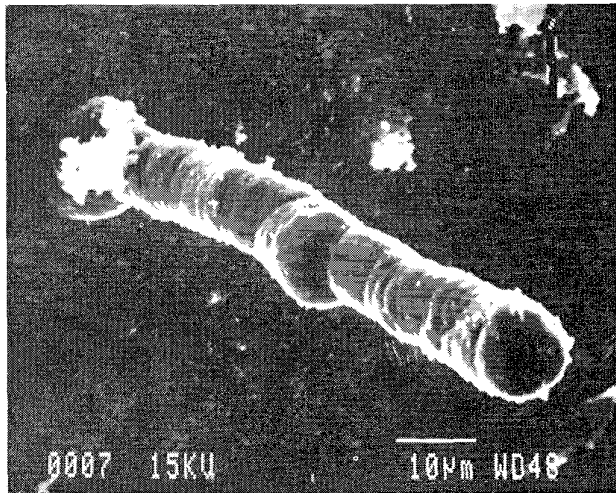


Fig. 7. Nickel column (10  $\mu\text{m}$  diameter).

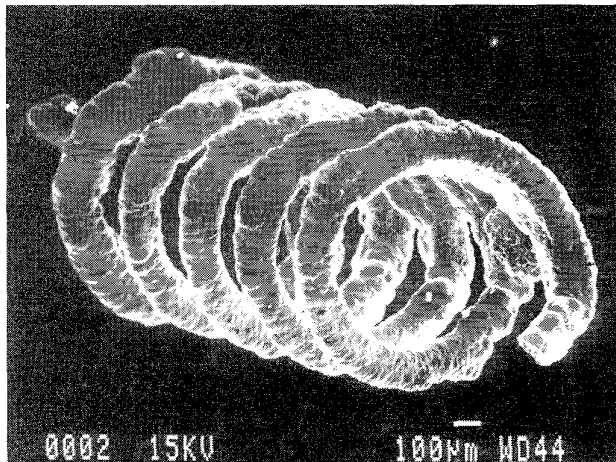


Fig. 8. Nickel spring.

to an asymmetry in the electrode, where a sharp tip protrudes at right angles to the shaft. In open loop mode, the deposition

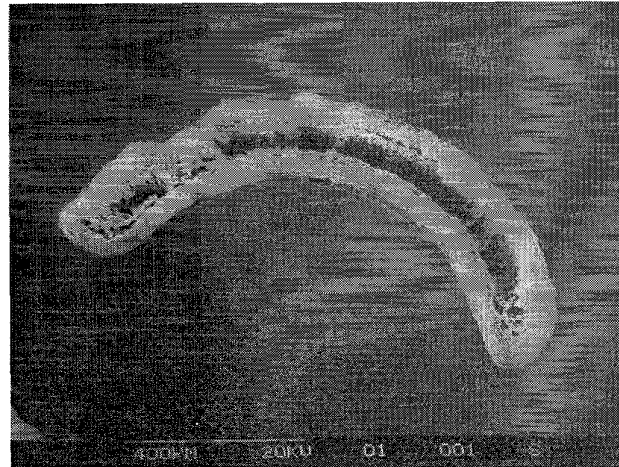


Fig. 9. Cross section of a spring loop revealing a hollow interior.

rate is faster than tip movement, and thus, the deposit tends to envelop the tip, possibly resulting in a hollow interior. It is also possible that the sharp tip, with its concentrated field, results in high local depletion of ions, favoring growth in the surrounding regions. Also, bubbles will preferentially form at the tip, potentially impeding growth.

The spring's modulus of elasticity was calculated using a measurement of the spring constant. A silicon beam force sensor (SensoNor AE801, Horten Norway) was mounted on a micro-stepping motor driven stage and the spring was compressed by 100  $\mu\text{m}$ . The spring constant was found to be 1.3 kN/m. Given the spring constant,  $k$ , spring diameter,  $d$  ( $170 \pm 25 \mu\text{m}$ ), number of turns,  $n = 6$ , and radius,  $R$  ( $500 \pm 25 \mu\text{m}$ ), the shear modulus,  $G$ , is [35]

$$G = \frac{64knR^3}{d^4} \quad (7)$$

and using Poisson's ratio,  $\mu = 0.3$  [35], modulus of elasticity,  $E$ , is

$$E = 2G(1 + \mu) \quad (8)$$

yielding a modulus of elasticity of  $200 \pm 120 \text{ GPa}$ . A typical value for polycrystalline nickel is 211 GPa [35]. The large uncertainty in the result is due to uncertainty in the spring wire diameter, on which the modulus depends to the fourth power. An X-ray diffraction spectrum [36], shown in Fig. 10, demonstrates that the deposited material is in fact polycrystalline nickel. Vertical bars indicate the positions and magnitudes of peaks expected for polycrystalline nickel.

High electro-deposition rates can be associated with hydrogen embrittlement, formation of voids as well as high residual stress in the resulting structures. Hydrogen embrittlement and residual stresses can be removed by annealing. Voids are clearly present around the core of the spring, as seen in Fig. 9, while the surrounding material is relatively void free. Thorough investigation of material properties is hampered by the irregular surface of the larger diameter deposits.

Good deposit material properties can be ensured by providing sufficient mass transport to the growth region, as has

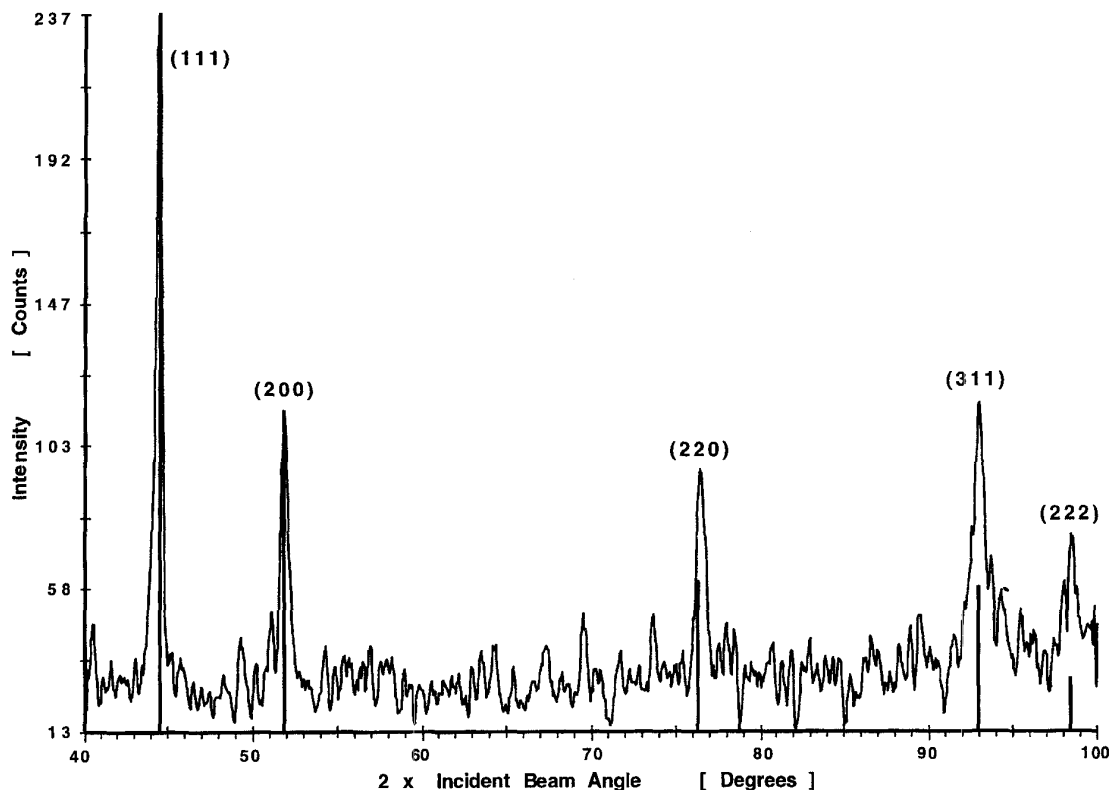


Fig. 10. X-ray diffraction spectrum from the spring showing peaks characteristic of polycrystalline nickel. Vertical lines indicate positions and amplitudes of peaks expected for polycrystalline nickel.

been demonstrated in laser enhanced electroplating and jet-plating [18]. We believe that, should it be necessary, material properties can be enhanced in the technique described here and surface finish improved by injecting ions into the growth region, either by forced convection, as in jet plating, or by local heating, as in laser-enhanced electroplating.

Thus far we have concentrated on building columns and wires. The next stage is to construct walls and solids. Fig. 11 shows the first attempt at building a wall. It is 60  $\mu\text{m}$  high, 500  $\mu\text{m}$  long, and approximately 15  $\mu\text{m}$  wide. To build the wall, the electrode tip was scanned horizontally, moving vertically in 3- $\mu\text{m}$  increments after each pass.

Microfabrication by localized electrodeposition promises to enable truly 3-D microfabrication from a range of materials, including metals, conducting polymers, and semiconductors, at low cost and with high resolution. Improving resolution is dependent on an ability to construct sufficiently small electrodes and, ultimately, on the minimum stable deposit size. It has already been demonstrated that submicrometer tips can be fabricated and employed to electrodeposit submicrometer-wide lines of material [16]. The key to successfully building in 3-D at these scales is feedback between the tip and the growing surface in order both to maintain resolution and determine surface geometry. While the current feedback method works and is very simple, some deformation is inevitable when the tip is initially lowered to contact the substrate. At kilohertz

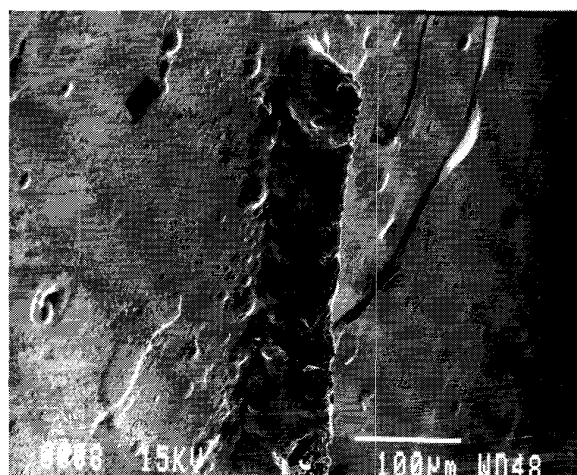


Fig. 11. Nickel wall.

frequencies, the electrolyte impedance is mostly resistive and current changes as a function of tip to surface distance. This effect is being investigated as a feedback mechanism.

## V. CONCLUSION

The concept of localized electrochemical deposition has been demonstrated and nickel micro-structures have been built.

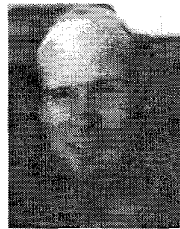
Electrodeposition is spatially constrained by limiting the extent of the electric field, which in turn localizes the deposit. Polycrystalline nickel is electrodeposited at rates two orders of magnitude faster than those of conventional electroforming, the rate enhancement likely the result of local convection induced by vigorous bubble formation. Fabricated structures include a multi-coiled helical spring and a 100- $\mu\text{m}$ -high, 10- $\mu\text{m}$ -diameter column. Results from two-dimensional selective electrodeposition processes suggest that 3-D electro-deposition with submicrometer spatial resolution is feasible.

#### ACKNOWLEDGMENT

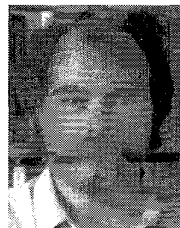
The authors are indebted to H. Campbell at McGill University and P. Kearney and J. Abdullah at M.I.T. for the S.E.M. micrographs as well as to J. Adario, who provided the x-ray diffraction spectrum. They also wish to thank C. Brennan, P. Madden, and S. Lafontaine very much for their helpful advice.

#### REFERENCES

- [1] J. Bryzek, K. Petersen, and W. McCulley, "Micromachines on the March," *IEEE Spectrum*, pp. 20-31, May 1994.
- [2] I. W. Hunter *et al.*, "A teleoperated microsurgical robot and associated virtual environment for eye surgery," *Presence*, vol. 2, pp. 265-280, 1993.
- [3] A. Rogner *et al.*, "LIGA technique—What are the new opportunities?," *J. Micromech. Microeng.*, vol. 2, pp. 133-140, 1992.
- [4] H. Guckel, T. R. Christenson, K. J. Skrobis, T. S. Jung, J. Klein, K. V. Hartojo, and I. Widjaja, "A first functional current excited planar rotational magnetic micromotor," in *Proc. IEEE Micro Electro Mechanical Syst.*, Fort Lauderdale, FL, 1993, pp. 7-11.
- [5] A. B. Frazier and M. G. Allen, "Metallic microstructures fabricated using photosensitive polyimide electroplating moulds" *J. Microelectromechanical Syst.*, vol. 2, p. 87-94, 1993.
- [6] M. Harmening *et al.*, "Moulding of three dimensional microstructures by the LIGA process," in *Proc. IEEE Micro Electro Mechanical Syst.*, Travemünde, Germany, 1992, pp. 202-207.
- [7] L. S. Van Dyke, C. J. Brumlik, and C. R. Martin, "UV laser ablation of electronically conductive polymers," *Synthetic Metals*, vol. 52, pp. 299-304, 1992.
- [8] C.-L. Kuo, T. Masuzawa, and M. Fujino, "High precision micronozzle fabrication" in *Proc. IEEE Micro Electro Mechanical Syst.*, Travemünde, Germany, 1992, pp. 116-121.
- [9] R. Dizon, H. Han, A. G. Russell, and M. L. Reed, "An ion milling pattern transfer technique for fabrication of three-dimensional micromechanical structures," *J. Microelectromechanical Syst.*, vol. 2, pp. 151-159, 1993.
- [10] F. T. Wallenberger and M. Boman, "Inorganic fibers and microstructures directly from the vapour phase," *Composites Science and Technology*, vol. 51, pp. 193-212, 1994.
- [11] K. Ikuta, K. Hirowatari, and T. Ogata, "Three dimensional micro integrated fluid systems (MIFS) fabricated by stereo lithography," in *Proc. IEEE Micro Electro Mechanical Syst.*, Oiso, Japan, 1994, pp. 1-6.
- [12] M. Boman and H. Westberg, "Helical microstructures grown by laser assisted chemical vapour deposition," in *Proc. IEEE Micro Electro Mechanical Syst.*, Travemünde, Germany, 1992, pp. 162-167.
- [13] W. H. Brünger and K. T. Kohlman, "E-beam induced fabrication of microstructures," in *Proc. Micro Electro Mechanical Syst.*, Travemünde, Germany, 1992, pp. 168-170.
- [14] P. G. Blauner, J. S. Ro, Y. Butt, and J. Melngaillis, "Focused ion beam fabrication of submicron gold structures," *J. Vacuum Sci. Technol.*, vol. B7, no. 4, pp. 609-617, 1989.
- [15] A. J. Bard, O. E. Hüsser, and D. H. Craston, "High resolution deposition and etching in polymer films," U.S. Patent 4968 390, Nov. 6, 1990.
- [16] J. Schneir, P. K. Hansma, V. Elings, J. Gurley, K. Wickramasinghe, and R. Sonnenfeld, "Creating and observing surface features with a scanning tunneling microscope," *SPIE* vol. 897, pp. 16-19, 1988.
- [17] Y.-M. Wu, F.-R. F. Fan, and A. J. Bard, "High resolution deposition of polyaniline on pt with the scanning electrochemical microscope," *J. Electrochem. Soc.*, vol. 136, pp. 885-886, 1989.
- [18] M. H. Gelchinski *et al.*, "Laser enhanced jet-plating and jet-etching," U.S. Patent 4497 692, Feb. 5, 1985.
- [19] R. L. McCarley, S. A. Hendricks, and A. J. Bard, "Controlled nanofabrication of highly oriented pyrolytic graphite with the scanning tunneling microscope," *J. Physical Chemistry*, vol. 96, pp. 10 089-10 092, 1992.
- [20] Southampton Electrochemistry Group, *Instrumental Methods in Electrochemistry*. New York: Wiley, 1985.
- [21] P. W. Atkins, *Physical Chemistry*, 4th ed. New York: Freeman, 1990.
- [22] A. J. Bard and R. Faulkner, *Electrochemical Methods: Fundamentals and Applications*. New York: Wiley, 1980.
- [23] F. A. Lowenheim, *Electroplating*. New York: McGraw-Hill, 1978.
- [24] R. M. Wightman and D. O. Wipf, "Voltammetry at ultramicroelectrodes," *Electroanalytical Chemistry*, vol. 15, pp. 267-353, 1989.
- [25] *Canning Handbook on Electroplating*, Birmingham, U.K.: W. Canning, 1978.
- [26] E. Raub and K. Muller, *Fundamentals of Metal Deposition*. New York: Elsevier, 1967, p. 46.
- [27] R. J. von Gutfeld, R. E. Acosta, and L. T. Romankiw, "Laser-enhanced plating and etching: mechanisms and applications," *IBM J. Research and Development*, vol. 26, pp. 136-144, 1982.
- [28] J. Cl. Puipe, R. E. Acosta and R. J. von Gutfeld, "Investigation of laser-enhanced electroplating mechanisms," *J. Electrochemical Society: Electrochemical Science and Technology*, vol. 128, pp. 2539-2545, 1981.
- [29] J. D. Jackson, *Classical Electrodynamics*, 2nd ed. New York: Wiley, 1975.
- [30] M. Fotino, "Tip sharpening by normal and reverse electrochemical etching," *Rev. Scientific Instruments*, vol. 64, pp. 159-167, 1993.
- [31] A. A. Gewirth, D. H. Craston, and A. J. Bard, "Fabrication and characterization of microtips for in situ scanning tunneling microscopy," *J. Electroanalytical Chemistry*, vol. 261, pp. 477-482, 1989.
- [32] M. V. Mirkin, F.-R. F. Ren, and A. J. Bard, "Scanning electrochemical microscopy part 13—Evaluation of the tip shapes of nanometer size microelectrodes," *J. Electroanalytical Chemistry*, vol. 328, pp. 47-62, 1992.
- [33] J. R. Brauer and B. E. MacNeal, *MSC EMAS User's Manual*, MacNeal-Schwender Corp., 1991.
- [34] G. Petzow, *Metalloraphic Etching*. New York: American Society for Metals, 1978, p. 45.
- [35] T. Baumeister, Ed., *Mark's Handbook*, 8th ed. New York: McGraw-Hill, 1979.
- [36] B. D. Cullity, *Elements of X-ray Diffraction*. Reading MA: Addison-Wesley, 1956, pp. 96-102.



**John D. Madden** is a graduate student in mechanical engineering at the Massachusetts Institute of Technology, Cambridge. His research is focused on developing microfabrication methods and conducting polymer actuators.



**Ian W. Hunter** is the D'Arbelloff Scholar and Associate Professor of Mechanical Engineering at the Massachusetts Institute of Technology, Cambridge, MA. His work is focused primarily on developing microbotic and microsurgical robotic systems, subsystems, and associated electrooptical mechanical instrumentation.